Use of Fragile Geologic Structures as Indicators of Unexceeded Ground Motions and Direct Constraints on Probabilistic Seismic Hazard Analysis

by Jack W. Baker, Norman A. Abrahamson, John W. Whitney, Mark P. Board, and Thomas C. Hanks

Abstract   We present a quantitative procedure for constraining probabilistic seismic hazard analysis results at a given site, based on the existence of fragile geologic structures at that site. We illustrate this procedure by analyzing precarious rocks and undamaged lithophysae at Yucca Mountain, Nevada. The key metric is the probability that the feature would have survived to the present day, assuming that the hazard results are correct. If the fragile geologic structure has an extremely low probability of having survived (which would be inconsistent with the observed survival of the structure), then the calculations illustrate how much the hazard would have to be reduced to result in a nonnegligible survival probability. The calculations are able to consider structures the predicted failure probabilities of which are a function of one or more ground-motion parameters, as well as structures that either rapidly or slowly evolved to their current state over time. These calculations are the only way to validate seismic hazard curves over long periods of time.

Introduction

For critical facilities, seismic hazard needs to be computed for ground motions with annual rates of exceedance of 10^{-6} (for nuclear power plants) to 10^{-9} (for nuclear waste repositories). At these low exceedance rates, very large ground-motion amplitudes are often predicted by standard probabilistic seismic hazard analysis (PSHA) procedures. This is in large part because ground-motion amplitudes for a given earthquake appear to be well represented by lognormal probability distributions, and extrapolating the lognormal distribution to a high number of standard deviations associated with extremely rare ground motions results in extremely large amplitudes. Because the lognormal distribution has no upper bound, there is no absolute upper bound to the ground-motion amplitudes that can be computed at very low probabilities.

An example of how these extreme ground motions arise in a standard PSHA is the 1998 Yucca Mountain Project PSHA (Stepp *et al.*, 2001). The hazard curves for peak ground acceleration (PGA) and peak ground velocity (PGV) in Figure 1 show progressively higher ground motions as they are extended to progressively lower rates of exceedance: at mean hazard levels of 10^{-6}/yr, 10^{-7}/yr, and 10^{-8}/yr, the corresponding PGAs are 3, 6, and 11g (Fig. 1a) and corresponding PGVs are 3, 6.5, and 13 m/s, respectively (Fig. 1b). These extreme ground motions, the consequence of extrapolating ground-motion distribution functions to extremely low

probability levels, have generated considerable consternation in the scientific, engineering, and regulatory communities: the upper end of these PGVs and PGAs has never been recorded for earthquakes, present exceptional challenges to the design and construction of facilities, and are regarded by many seismologists as "physically unrealizable" (e.g., Andrews *et al.*, 2007). These extreme PGV levels may be unrealizable because the amplitude of the ground motion traveling through a rock mass is limited by the shear strength of the rock mass through which it propagates. It is easy to say that the large ground motions predicted at low probability levels from the 1998 PSHA do not seem reasonable, but it is much more difficult to provide a technical basis for a reduced ground-motion value.

One source of evidence for a reduced ground-motion value comes in the form of fragile geologic structures such as precarious rocks, which would likely have been destroyed by seismic ground motions if the PSHA calculations are correct. Precarious rocks, also precariously balanced rocks (PBR) have been used as constraints on local ground motions since Brune and Whitney (1992) and Brune (1996) recognized PBRs as natural seismoscopes. PBRs are a subset of the more general class of fragile geologic structures (FGS), which speak to unexceeded ground motions (UGM), ground motions that would have damaged or destroyed any object, structure, or feature during the time in which it was fragile.
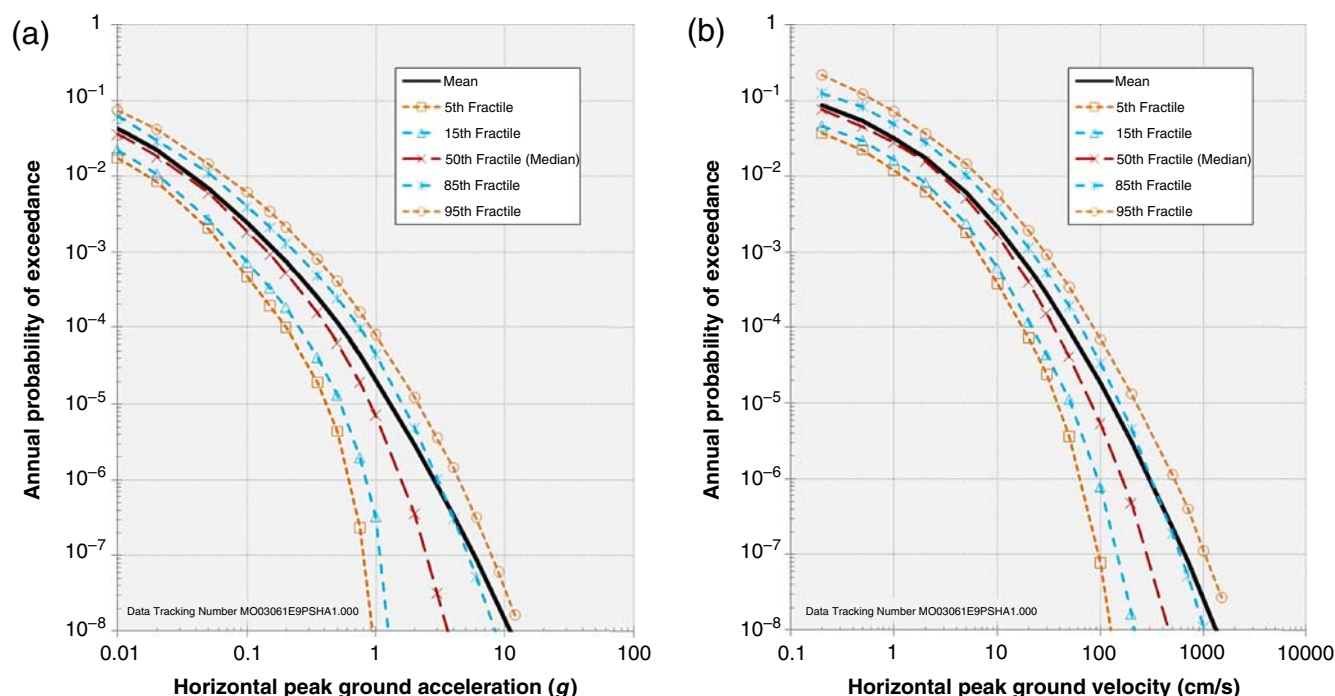
Figure 1. Example output from probabilistic seismic hazard analysis. (a) Horizontal PGA, and (b) horizontal PGV, at Point A, a hypothetical, reference rock outcrop site at the Yucca Mountain repository horizon (Stepp *et al.*, 2001). From the 1998 Yucca Mountain Project PSHA extended to 10^{-8}/yr by BSC (2005). The color version of this figure is available only in the electronic edition.

Such FGS include natural bridges and arches, liquefiable deposits, hoo-doos, precipitous slopes and cliffs, and lithophysal cavities, as well as PBRs. Lithophysae (delicate voids and crystals in welded vesicular tuff–literally, rock bubbles) are the result of gases exsolving from cooling lava flows and ashfall tuffs. PBRs are the most important of the FGS because they occur widely across active tectonic terrains of the southwestern United States (e.g., Brune, 1996; O'Connell *et al.*, 2007; Purvance *et al.*, 2008) and elsewhere in the world (e.g., Stirling and Anooshehpoor, 2006).

When used as a constraint for PSHA, one needs to know the "fragility age" of the FGS of interest (i.e., the amount of time it has been in its presently precarious/fragile state) as well as the ground motions that, had they occurred, would have damaged or destroyed it. Early work used the presence of desert varnish on PBRs to indicate fragility ages of thousands of years or greater and quasistatic estimates of toppling accelerations to approximate a PGA that had not occurred in the fragility age of the PBR. As recounted in Anderson *et al.* (2011), techniques for estimating both the fragility ages and toppling motions have advanced considerably in the past decade to include cosmogenic dating of features (Balco *et al.*, 2011) and numerical modeling of dynamic toppling behavior (Purvance *et al.*, 2009).

The Points-in-Hazard-Space approach and graphic developed in the course of the Extreme Ground Motions research program (Anderson and Brune, 1999; Abrahamson and Hanks, 2008; Hanks and Abrahamson, 2008) allows one to compare PBR constraints directly with seismic hazard curves, the specific place and application being Yucca Mountain, Nevada. Reciprocal fragility ages were used to approximate the probabilities of nonexceedance of estimates of PGV that would have toppled the PBR, had they occurred. This simple approach, although effective in demonstrating that the seismic hazard at Yucca Mountain had been significantly overstated, lacked the quantitative probabilistic framework we develop in this paper.

This paper provides a description of the types of evidence that have been compared to PSHA results and describes a probabilistic procedure for performing such comparisons. The proposed calculations can incorporate uncertainty in the age and fragility of the observed geologic structure, so as to be consistent with other uncertainties used to perform the initial seismic hazard analysis computation.

Seismic Hazard Analysis

Standard PSHA is performed using a seismic source characterization that describes the rates of occurrence of all earthquake events in the region and using a ground-motion prediction model to predict the distribution of ground-motion intensities for each earthquake event. Those two models capture inherent physical variability ("aleatory" variability) in the processes that generate ground motions at a given site. We do not have perfect seismic source characterization models or ground-motion prediction models, however, so typically a logic tree is used to describe our lack of knowledge ("epistemic" uncertainty) in the proper model by proposing a list of plausible models via a logic tree, along with

weights representing our degree of belief in each model (SSHAC, 1997; Abrahamson and Bommer, 2005; McGuire et al., 2005).

The output of such a calculation is a plot (as shown in Fig. 1) that shows mean hazard curves and fractiles for PGA and PGV. An important feature of these calculations is that there is generally no upper bound on the ground-motion predictions, so there is no fixed upper limit on the amplitudes of predicted ground motions (although large amplitudes may be extremely infrequent).

Potential Constraints on Hazard Curves

Three general types of constraints have been proposed to constrain PSHA predictions of large ground-motion intensities: physical limits on ground motion, truncation of ground-motion predictions, and unexceeded ground motions associated with fragile geologic structures (Hanks et al., 2006).

A physical limit to earthquake ground motion is a constraint such that motions larger than this limit cannot occur ever. Such a limit, if it can be plausibly demonstrated and calculated, provides a clear bound on extreme ground motions. Physical limits might arise from the limited strength of rocks at the site of interest or anywhere along the path between the rupture and the site. The strength of rocks increases with confining pressure, so we may expect that rock properties at or near the site will place more stringent limits on ground motions than will rock properties at midcrustal depths, where the earthquakes occur. Moreover, rocks at shallow depth are easily accessible, allowing for both *in situ* observation of their structure and fabric as well as sampling for laboratory testing. Rock mechanics can then be used to identify limits at which rock fracture would occur (BSC, 2005, Section B.2.2; Lockner and Morrow, 2008). Physical limits to ground motion might also arise from limits on the source excitation of crustal earthquakes, but these are difficult to discern with confidence given the inaccessibility of earthquake sources and the short record of instrumental recordings. A related approach is to identify a hard limit on intensities that have zero probability of being exceeded under any condition using numerical simulations, a challenging but feasible approach (Andrews et al., 2007). Physical limits do appear to provide useful constraints on extreme ground motions, but are not addressed further here.

A second potential approach to constrain hazard is to truncate predictions of ground motions at a fixed number of standard deviations ("epsilons") above the median prediction for a given earthquake scenario. This approach is problematic because the truncation point is arbitrary and not supported by observational evidence and because the truncation is with respect to a model prediction rather than with respect to an absolute ground-motion intensity value where some physical phenomenon produces the truncation. The problems with this approach are described in detail by Bommer et al. (2004), and thus this line of thinking has not produced defensible constraints on extreme ground motion.

A third approach is to use the existence of a fragile geologic structure as an indicator that ground motions with amplitudes large enough to fail the structure have not occurred during its lifetime. Examples of features that indicate unexceeded ground motions include undamaged lithophysae (rock bubbles) and precariously balanced rocks. Although these observations provide clear qualitative evidence, several challenges are associated with using them for quantitative comparisons to probabilistic seismic hazard calculations. These challenges will be addressed below.

Using Fragile Geologic Structures to Constrain Hazard

FGS are indicators of UGM—ground motions strong enough to drive an FGS to failure but which have not occurred during the time period for which the FGS has indeed been fragile. These structures provide observations in a single window of time from the origin of the structure until present, whereas hazard curves quantify long-term rates of exceedance of ground-motion amplitudes. There is also uncertainty in the amplitude of ground motion that would destroy those structures. For these reasons, it is not straightforward to compute the UGM associated with an FGS.

To illustrate the proposed approach to address these challenges, we first consider the Topopah Spring tuff formation that underlies Yucca Mountain and is the host horizon for the underground repository. It consists of ~300 m of silica-rich, densely welded, pyroclastic flow units laid down 12.8 million years ago and contains distinctive upper (Tptpul) and lower (Tptpll) lithophysal units. Lithophysae are cavities that form in pyroclastic flows and volcanic tuffs as a result of the volcanic gases exsolved during the cooling process but contained within the cooling rock mass. The cooling occurred over a relatively short period of time compared to the age of the units, so the age of the lithophysae can be taken as 12.8 million years without concern for the fragility varying over that time period.

Tptpul lithophysae tend to be roughly spherical, uniform in size and distribution, and small in dimension (diameters of 1–10 cm); the matrix material is largely unfractured. Tptpll lithophysae are more irregular in shape, size, and distribution, as seen in Figure 2. Lithophysae range in size from about 1 cm to nearly 2 m in dimension and have spacing that ranges from about 10 to 50 cm, although they may be more closely spaced in local regions. The shapes range from elliptical or spherical to irregular, cuspate and merged cross sections, or elongate along fractures. The matrix between lithophysae often has a fabric of short length (< 1 m) and discontinuous cooling fractures that have a primarily vertical orientation. These fractures typically are not interconnected and do not intersect lithophysal cavities. The overall porosity of Tptpll due to the lithophysae is ~20%, and these cavities constitute 10%–30% of the rock volume, thus weakening
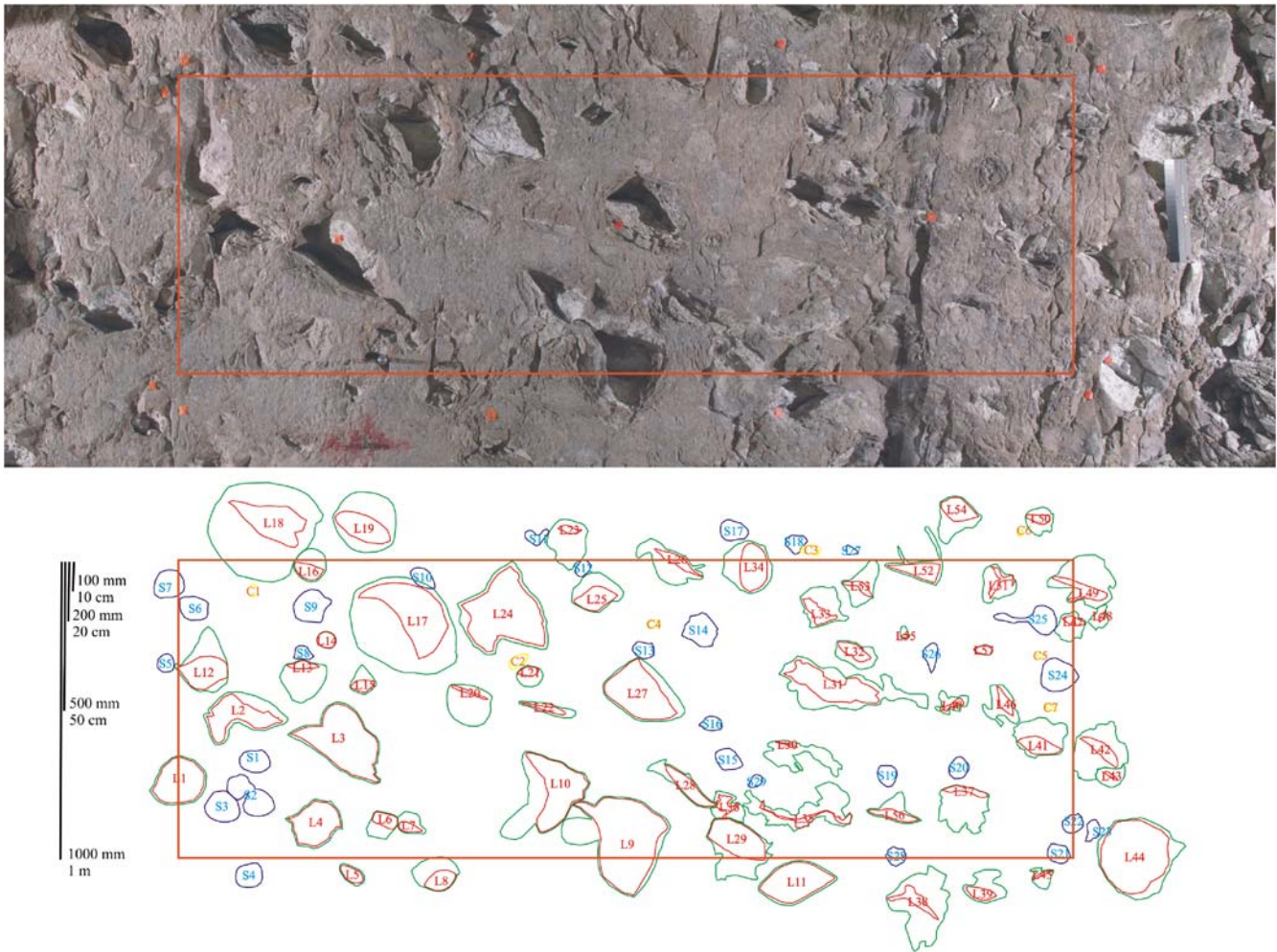
Figure 2. Photograph and panel map (3 × 1 m) from the ECRB tunnel sidewall in Tptpll, showing traces of lithophysal cavities and vapor-phase alteration rims. The color version of this figure is available only in the electronic edition.

the rock considerably with respect to the passage of seismic waves. Very few of these lithophysae are cut by cooling fractures or joints, and none shows appreciable effects of damage, offsets, or collapse that can be attributed to the passage of seismic waves.

Elastic properties, compressive strength, and failure strains were determined by laboratory testing for large samples (up to 288 mm in diameter) of the lithophysal units (BSC, 2005). These data were used to estimate the "threshold shear strain" that would result in geologically observable damage to the lithophysal units. Two alternative models relating strain and PGV were then estimated from the site response studies, one (Upper Mean Tuff) being based on more linear material response to incoming ground motion and the other (Lower Mean Tuff) based on more nonlinear behavior, Appendix III). The derivation of these fragility curves was complex but is well documented elsewhere. Here we take them as a given for the purpose of demonstrating computation of an unexceeded ground motion. The resulting fragility functions, which specify the failure probability of the object

of interest as a function of some ground-motion parameter such as PGV, are shown in Figure 3.

Using a fragility function and a hazard curve for the site, we can calculate the probability that a given feature would fail in any one-year period of time. $P_{\text{annual}}(G_{\text{fails}})$ is the sum of the products of the rate of occurrence of ground motion and the conditional probability of failure, given the ground motion. The annual hazard curve $\nu(z)$ gives the mean rate of exceedance of scalar ground motion z, and its derivative with respect to z gives the rate of occurrence of z. The annual probability of failure is then given by

$$
\begin{aligned}
P_{\text{annual}}(G_{\text{fails}}) &= \int P(G_{\text{fails}}|\text{PGV} = z_i)\left|\frac{d\nu(z)}{dz}\right|dz \\
&= \sum_i P(G_{\text{fails}}|\text{PGV} = z_i)P_{\text{annual}}(\text{PGV} = z_i),
\end{aligned}
$$

(1)

where G_{fails} is the event that the FGS fails, $P(G_{\text{fails}}|\text{PGV} = z)$ is the probability that the FGS fails, conditional on occurrence
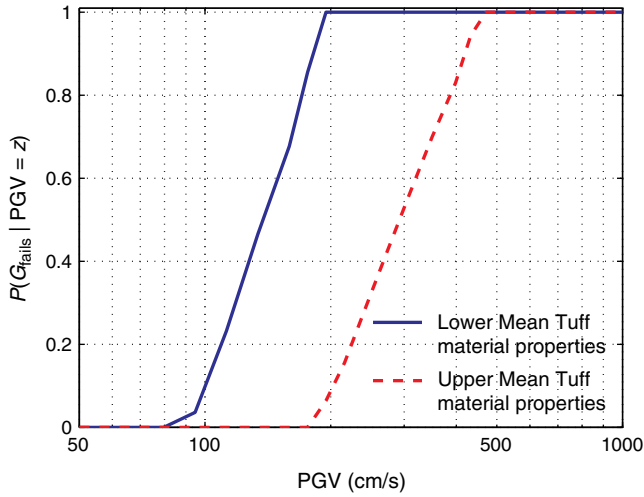
Figure 3. Fragility curves as expressed by the Upper and Lower Mean Tuff properties. The color version of this figure is available only in the electronic edition.
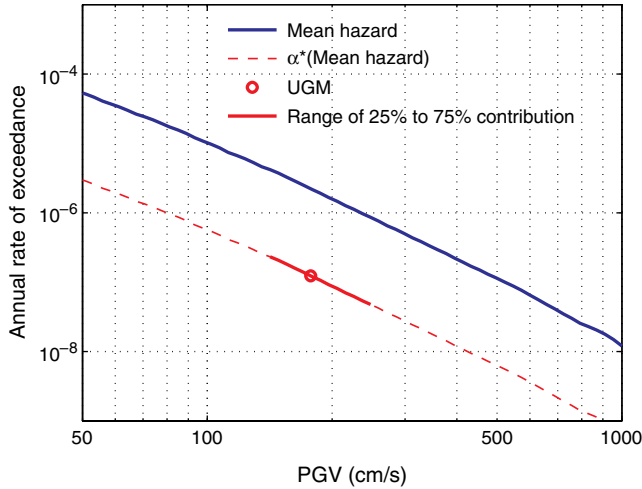
Figure 4. Original mean hazard curve for the site and adjustment of hazard curve to correspond to a 5% survival probability of the lithophysae. The color version of this figure is available only in the electronic edition.

of a ground motion with PGV $= z$ (the FGS "fragility function"), and "|" is used to denote conditioning. The calculation can be specified in continuous form as indicated by the integral in equation (1), but in practice it is evaluated numerically by discretizing the continuous range of PGV values of interest and summing over those values, z_i. Figure 3 shows two fragility functions for the lithophysal units, and Figure 4 shows the Yucca Mountain mean hazard curve with respect to PGV. For this hazard and the Lower Mean Tuff fragility curve shown above, $P_{\text{annual}}(G_{\text{fails}}) = 4.5 \times 10^{-6}/\text{yr}$.

Given the above annual failure probability, the probability of surviving for one year is $1 - P_{\text{Annual}}(G_{\text{fails}})$, and the probability of surviving for T years (assuming potential failures in each year are mutually independent) is

$$P(G_{\text{not failed}}) = [1 - P_{\text{annual}}(G_{\text{fails}})]^T. \quad (2)$$

For the hazard curve and Lower Mean Tuff fragility above, and a 12.8 million year age of the Tuff, this probability is 10^{-25} or, for all practical purposes, zero. This contradicts the observed existence of the structure, suggesting that the hazard curve is overpredicting the rate of exceedance of the large PGV values that would cause failure of this FGS. The approach proposed here to reconcile such a contradiction is to multiply all rates of exceedance from the original hazard curve by a constant α, so that if the original hazard curve was $\nu(z)$, the adjusted hazard is $\alpha\nu(z)$. By inspection of equation (1), we can see that this will modify the annual failure probability of the structure by the same constant. We can, thus, determine the scale factor α to be applied to the hazard curve that would lead to a specified probability P_1, for which our structure does not fail during its lifetime. For a structure that has been fragile for T years, P_1 is

$$P_1 = [1 - \alpha_{P_1} P_{\text{annual}}(G_{\text{fails}})]^T. \quad (3)$$

If we are interested in the hazard curve that would lead to a 5% probability of the FGS not failing, we can substitute $P_1 = 0.05$ and solve for the corresponding α_{P_1}

$$\alpha_{0.05} = \frac{1 - 0.05^{1/T}}{P_{\text{annual}}(G_{\text{fails}})}. \quad (4)$$

For this example, $\alpha_{0.05} = 1/19$, Figure 4 shows the resulting scaled hazard curve as a dashed line. For any hazard curve above this scaled hazard, there is $<5\%$ chance that the geologic structure would have survived in its existing state of fragility for $T = 12.8$ million years. The 5% target is a choice in this analysis and is addressed in the Discussion section below.

We can further analyze the results from the calculations above to identify which particular PGV values are contributing most to failures of the structure. The product of the rate of occurrence of a given PGV and the corresponding fragility (the integrand of equation 1) provides the contribution of each PGV to the total failure probability of the fragile geologic structure. These contributions are computed as follows and plotted in Figure 5a

$$P(G_{\text{fails}} \text{ due to PGV} = z_i) = \frac{P(G_{\text{fails}}|\text{PGV} = z_i)P_{\text{annual}}(\text{PGV} = z_i)}{P_{\text{annual}}(G_{\text{fails}})}. \quad (5)$$

We can also compute the cumulative contribution of all PGVs $\leq z$ to failure, which is computed as follows and plotted in Figure 5b

$$P(G_{\text{fails}} \text{ due to PGV} \leq z) = \frac{\sum_{z_i=0}^{z} P(G_{\text{fails}}|\text{PGV} = z_i)P_{\text{annual}}(\text{PGV} = z_i)}{P_{\text{annual}}(G_{\text{fails}})}. \quad (6)$$

(a)

(b)
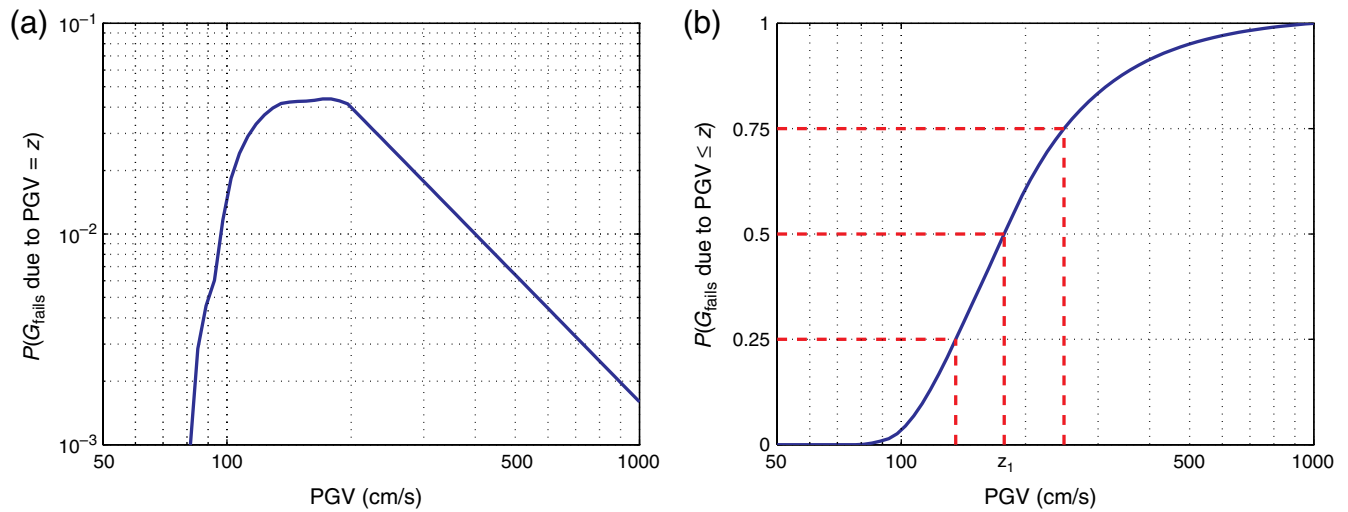
Figure 5. (a) Contribution of PGVs to failures of the feature. (b) Cumulative contributions of PGV $\leq z$ to failures of the feature. The color version of this figure is available only in the electronic edition.
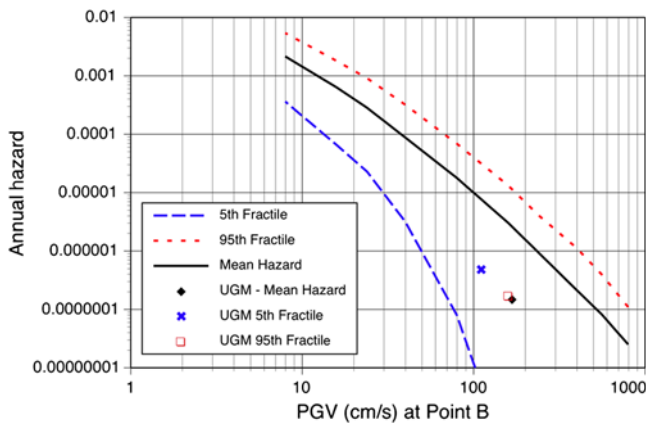
Figure 6. Effect of different slopes of the hazard curves on the UGM. The color version of this figure is available only in the electronic edition.

The median of the PGVs contributing to failure, denoted z_1, is taken as the UGM for this fragile geologic structure. The 50th percentile cumulative failure probability point on the scaled hazard curve fixed by z_1 is the PGV most strongly constrained by the fragile geologic structure. This z_1 value is shown in Figure 4, along with a solid red segment of the scaled hazard curve indicating the range of PGV that covers the 25%–75% range of the failure probability in Figure 5b, revealing that the fragile geologic structure constrains only part of the hazard curve (this range is chosen to illustrate that there is not just a single PGV value for which the FGS is providing some constraint). This point tells us the following: if the hazard curve passes through this point, then there is a 5% probability that the structure would survive T years without failing, and this is the median of the PGV values that would cause failure of the structure.

The relative values of z_1 and the point of 50% probability of failure depend on the slopes of the hazard curve and the fragility curve. Typically, z_1 is lower than the ground motion at the 50% failure probability because there are so many more small earthquakes with smaller ground motion; even though the fragility is low, the rates of the smaller PGVs are much higher than the rates of ground motions corresponding to the 50% failure probability on the fragility function. If the fragility curve is steep (e.g., the fragile geologic structure is brittle), then the z_1 value will be close to the value that leads to a 50% chance of failure because the fragility for the lower ground-motion values will be very small, offsetting the higher rate of occurrence of the smaller ground-motion values.

With this approach, the absolute level of the original hazard curve does not affect the location of the UGM. If two hazard curves differ only by a multiplicative factor on their rates (i.e., they have the same shape), then z_1 as determined by this method is unchanged and α simply adjusts for the differences in levels of the original hazard curves. The location of the UGM will depend upon the slope of the hazard curve, however, as the slope tells us the relative rates of large and small PGV, and differences in these relative rates will affect the PGV values that most constrain the hazard curve.

As an example of the dependence of the UGM point on the hazard curve, the UGM is shown for three different PGV hazard curves in Figure 6: mean, 95th fractile, and 5th fractile. For the mean and 95th fractile hazard curves, the shapes are similar and so there is almost no change in the location of the UGM. For the 5th fractile, the slope becomes much steeper, indicating that large PGV values are predicted to be very rare, so z_1 becomes smaller as the smaller PGVs thus provide the stronger constraint. The UGM based on the 5th fractile hazard is shifted up and to the left. All three points fall along a line following the general slope of the hazard curves, indicating that in all three cases the FGS provides a consistent evaluation of the hazard curve. Note that the
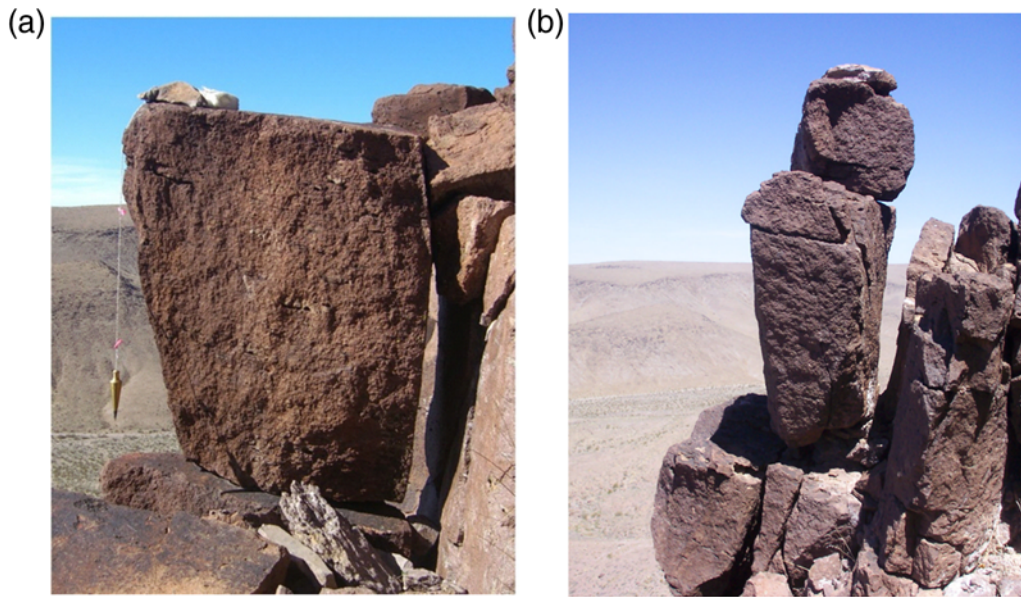
Figure 7.   (a) Photograph of PBR Matt-cubed. (b) Photograph of PBR Tripod. The color version of this figure is available only in the electronic edition.

5th fractile hazard curve lies below the UGM points, meaning that the FGS would have $>5\%$ chance of surviving if it were the true hazard curve. We note that fractile hazard curves are not necessarily representative of actual hazard curves from individual logic tree branches, but these calculations nonetheless serve to illustrate the role of the hazard curve slope on UGMs. Further, Figure 4 illustrated that the UGM is constrained by a relatively narrow range of PGV values for which the fractile hazard curve is likely similar to an individual hazard curve.

Fragile Geologic Structures with Vector Fragility

Many PBRs have been discovered and documented on the west face of Yucca Mountain and elsewhere (e.g., Brune and Whitney, 1992, 2000; Bell *et al.*, 1998; Anderson and Brune, 1999; Purvance *et al.*, 2008; Stirling *et al.*, 2010). These features have great potential to constrain seismic hazard calculations, but two complications arise when one is used to compute an unexceeded ground motion: its toppling probability is a function of both PGA and PGV, requiring knowledge of their joint probability distribution in a given future ground motion, and the rocks evolve in shape over time so that their fragilities are not constant over their lifetimes. To illustrate how these complications can be addressed, we perform an example evaluation of the PBR named Matt-cubed, located on the west face of Yucca Mountain. A photograph of this rock is shown in Figure 7a, and its fragility curve is shown in Figure 8a, as determined by Purvance *et al.* (2009). The derivation of this fragility curve was complex but is well documented elsewhere. Here we take it as a given for the purpose of demonstrating computation of an unexceeded ground motion.

This vector fragility causes a difficulty for the UGM computation because hazard curves provide the rate of occurrence of a given PGA or PGV individually and not the rate of jointly observing a given PGA and a given PGV in a single ground motion. To use the PBR toppling fragilities in the context of a UGM calculation, which considers PGV hazard only, we need to replace the functional dependence on PGA (which we do not know) with some equivalent information that we do know.

To begin, we first convert the pairs of PGA and PGV/PGA values calculated by Purvance *et al.* (2009) into pairs of PGV and PGA/PGV values, with PGV as the abscissa, as illustrated in Figure 8. Each coordinate in Figure 8a has some corresponding coordinate in Figure 8b, and the two corresponding coordinates have identical toppling probabilities. For a given PGV value, Figure 8b now provides failure probabilities as a function of PGA/PGV; this is illustrated in Figure 9 for PGV = 30 cm/s.

Earthquake seismologists will know that PGV has a strong magnitude dependence (e.g., McGarr and Fletcher, 2007) and so does PGA/PGV, although less strong as we shall see shortly. So how does PGA/PGV depend on M? This is shown empirically in Figure 10, which shows observed PGA/PGV values from ground motions on rock sites ($V_{S30} > 500$ m/s) at short distances ($R < 20$ km) from the Next Generation Attenuation data set (Chiou *et al.*, 2008). The mean value of ln(PGA/PGV) can be predicted as a function of magnitude using the following regression equation, which is also shown in Figure 10

$$E[\ln(\text{PGA}/\text{PGV})] = 6.08 - 0.534M - 0.074(M - 6.07)^2. \tag{7}$$

There is not a significant trend in this data with distance or V_{S30}, so the regression equation is not dependent on those
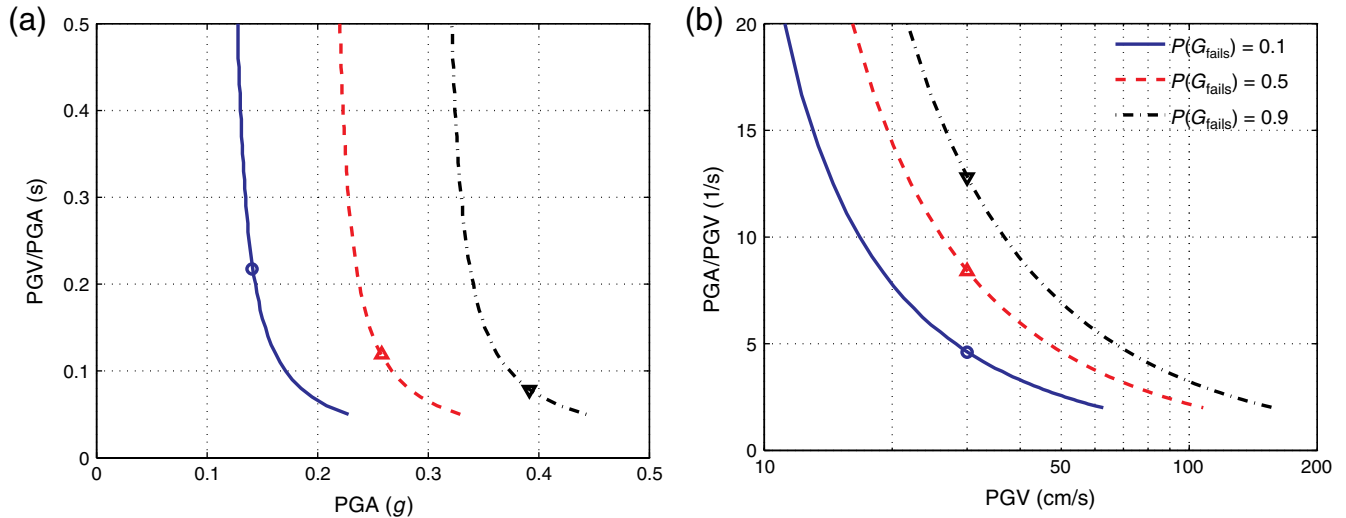
Figure 8. Overturning probabilities for the PBR Matt-cubed. (a) Plotted as a function of PGA and PGV/PGA. (b) Plotted as a function of PGV and PGA/PGV. The color version of this figure is available only in the electronic edition.
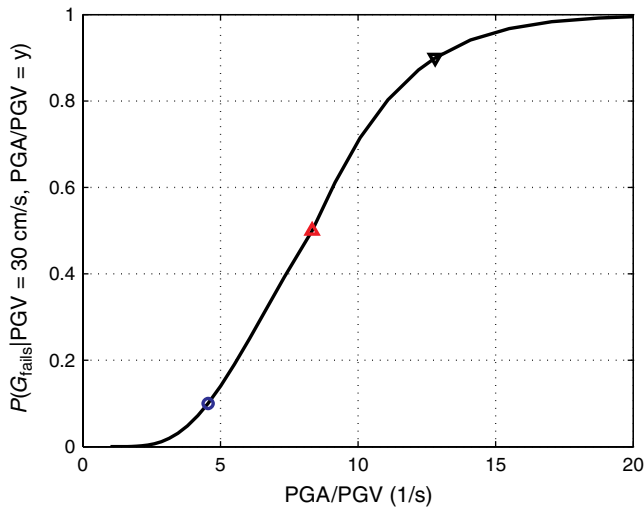
Figure 9. Overturning probabilities for the PBR Matt-cubed as a function of PGA/PGV, given PGV = 30 cm/s. The three points marked with symbols on this fragility curve correspond to the points with the same symbols in Figure 8. The color version of this figure is available only in the electronic edition.

Figure 10. Scaling of PGA/PGV with magnitude for rock sites ($V_{S30} > 500$ m/s) at short distances ($R < 20$ km). The color version of this figure is available only in the electronic edition.

variables. The standard deviation of prediction errors from this equation is 0.49. Assuming that PGV/PGA for a given magnitude is a lognormal random variable, the probability density function (PDF) for PGA/PGV, associated with a given magnitude M, is then

$$f_{\mathrm{PGA/PGV}}(y|M) = \frac{1}{0.49 y \sqrt{2\pi}}$$
$$\exp\left\{-0.5\left(\frac{\ln y - [6.08 - 0.534M - 0.074(M - 6.07)^2]}{0.49}\right)^2\right\}. \tag{8}$$

Figure 10 illustrates this PDF for $M = 6$ and $M = 7$.

Knowing the probability of failure of the PBR given a PGV and PGA/PGV pair, and the distribution of PGA/PGV values given an earthquake magnitude, we can integrate over all possible PGA/PGV values to obtain the probability of failure for every PGV and M (at the close distances implicit in Fig. 10)

$$P(G_{\mathrm{fails}}|\mathrm{PGV} = z, M = m) = \int P(G_{\mathrm{fails}}|\mathrm{PGV} = z,$$
$$\mathrm{PGA/PGV} = y) * f_{\mathrm{PGA/PGV}}(y|m) dy, \tag{9}$$

where $P(G_{\mathrm{fails}}|\mathrm{PGV}, M)$ is a generalized form of the fragility used in equation (1). These fragilities for the example rock are plotted in Figure 11 versus PGV for a range of magnitudes. This figure illustrates that large magnitude earthquakes require
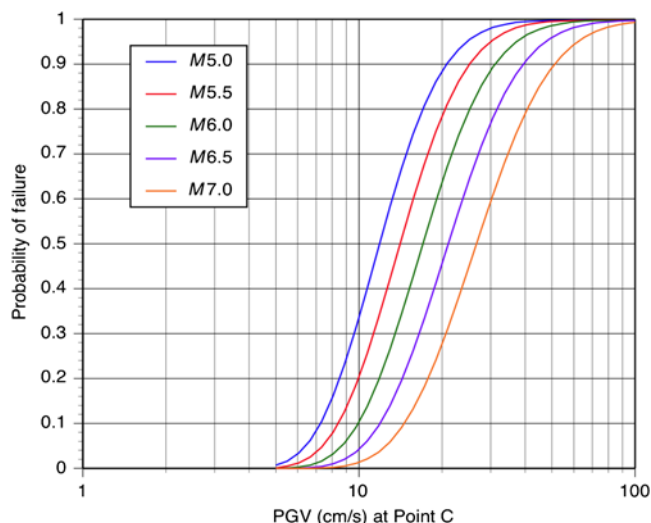
Figure 11. Variation of the PGV-based fragilities for PBR Matt-cubed, as a function of magnitude. The color version of this figure is available only in the electronic edition.

higher PGVs in general to topple the feature because their PGA values (relative to PGV) are smaller than for small-magnitude earthquakes with the same PGV.

This fragility function format is useful because we know the distribution of magnitudes associated with a given PGV value at the site from seismic hazard deaggregation calculations (e.g., McGuire, 1995). Here we denote the deaggregation probability that a ground motion with $PGV = z_i$ was caused by an earthquake with $M = m_j$ as $\mathrm{deagg}(m_j|z_i)$, noting that the deaggregation calculation typically discretizes the continuous range of possible magnitudes. Using this deaggregation information and the magnitude-dependent fragility function of equation (9), we can compute the annual probability of failure of the precarious rock using

$$P_{\mathrm{annual}}(G_{\mathrm{fails}}) = \sum_i \sum_j P(G_{\mathrm{fails}}|PGV = z_i, M = m_j)$$
$$\times \mathrm{deagg}(m_j|z_i)P_{\mathrm{annual}}(PGV = z_i). \quad (10)$$

This result can then be used to compute survival probabilities using equation (2), and the hazard curve can again be scaled by α to find a UGM associated with 5% survival probability of the FGS. One additional assumption required here when doing the hazard scaling is that the deaggregation probabilities $\mathrm{deagg}(m_j|z_i)$ would be unchanged by the scaling of the hazard curve.

With this procedure, we thus see that even vector fragility functions can be used to compute UGMs, if one can relate the vector of fragility function inputs to information related to the hazard curve (in this case, PGV and M).

Time-Varying Fragile Geologic Structures

In the previous sections, we considered fragile geologic structures having constant fragilities over their lifetime. This assumption is reasonable for fragile geologic features that form over a short time interval relative to their age, such as the lithophysal units. A structure formed by erosion or exhumation, however, will have a time-dependent fragility as it evolves from a more stable configuration to an increasingly more fragile one—until it fails (e.g., O'Connell et al., 2007).

An example of a time-dependent fragility is shown in Figure 12a. The time dependence of the fragility curves can be parameterized using the PGV that gives a 50% chance of failing the geologic feature, denoted PGV_{50}. We have two constraints on the time dependence of the fragility: the PGV_{50} value based on the current configuration, and the PGV_{50} value for a rock that has just become a free face. With respect to the PBRs on the west face of Yucca Mountain, we know that PGVs of 500 cm/s from underground nuclear
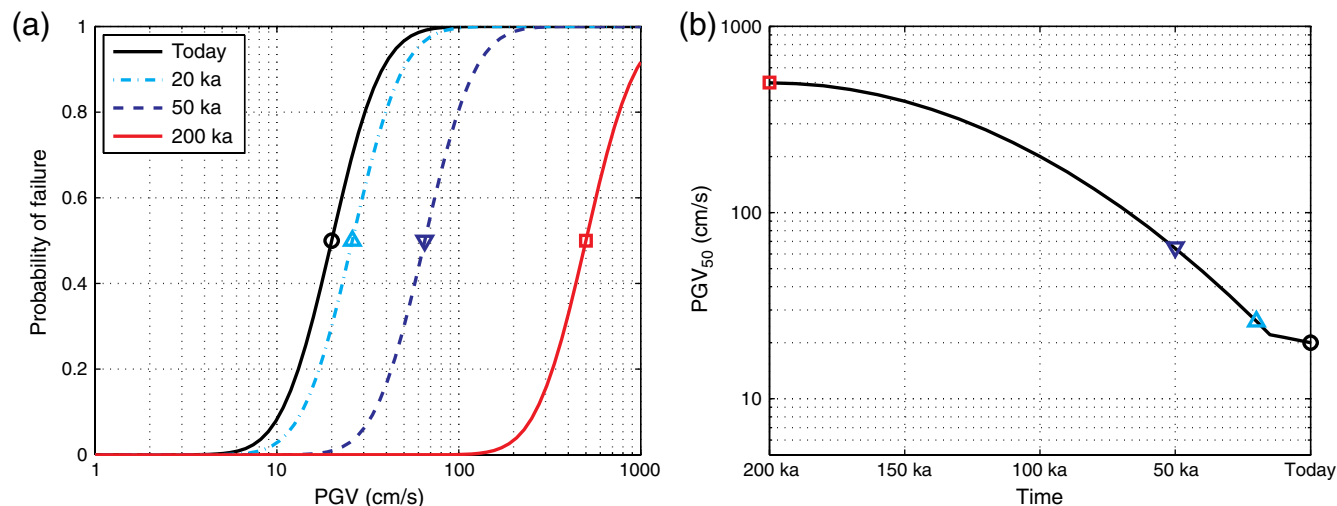
Figure 12. (a) A time-varying fragility function for a feature. (b) Median fragility value as a function of time. The color version of this figure is available only in the electronic edition.
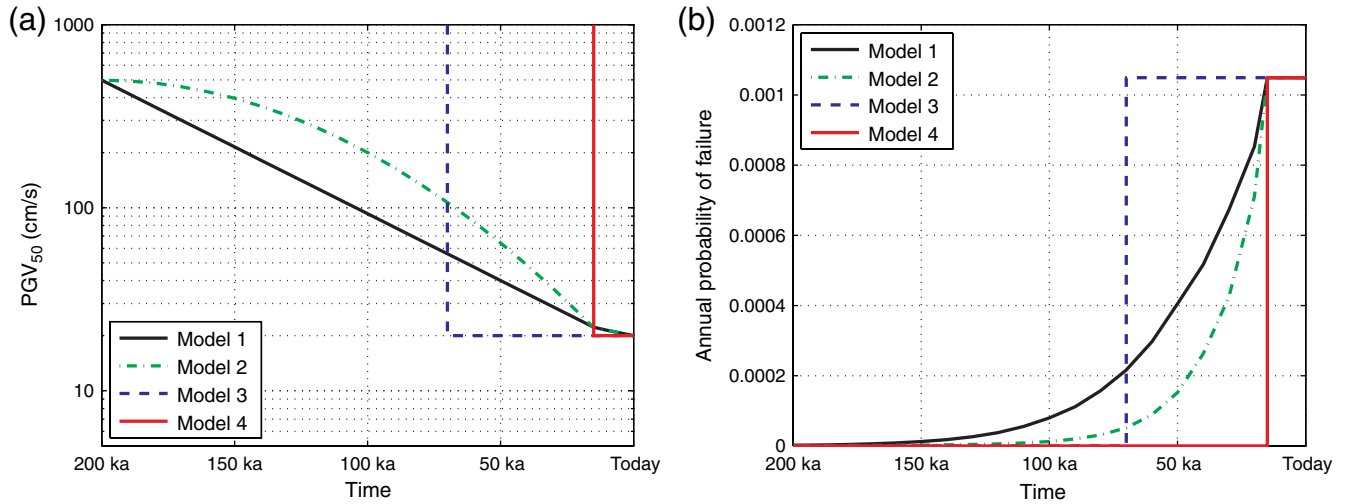
Figure 13. (a) Four models for time-varying median fragility. (b) Probability of failure in each year, given four time-varying fragility models. The color version of this figure is available only in the electronic edition.

explosions on Pahute Mesa cause massive cliff fracturing and failure (Brune *et al.*, 2003), so we choose this value for the PGV_{50} of newly exposed rock. We also know the present-day fragilities of the various PBRs. This evolution is sketched schematically in Figure 12b, parameterized in terms of PGV_{50}, the PGV that has a 50% chance of failing some PBR or precarious rock stack. At 200 ka, we suppose that the PBR has just been exposed and that a $PGV_{50} = 500$ cm/s is needed to topple it with 50% probability (this is hardly a precarious rock!). As erosion works away at the cooling joints and other fractures, PGV_{50} progressively decreases, such that at the present time PGV_{50} is only 20 cm/s. Here we assume that the log standard deviation of the fragility function is constant over its lifetime, but that parameter could also be varied in principle if needed.

To evaluate the effect of variations in the evolutionary model on the PBR's implied UGM, we consider four conceptual models shown in Figure 13a. Each model evolves from the intact cliff face to the current fragile feature today. Model 1 shows a linear decrease of $\log PGV_{50}$ with time, and model 2 shows a quadratic decrease of $\log PGV_{50}$ with time. Both models slow their decrease at 15 ka, incorporating the idea that the warmer, drier Holocene climate slowed the erosion rate over that time period. Model 3 assumes a fixed age of 70 ka for the PBR, and model 4 is functionally the same as model 3 but with an age of 15 ka. 70 ka is an approximate age of Matt-cubed determined from cosmogenic isotope dating, whereas 15 ka is a lower-bound age of the rock determined by varnish microlamination dating (Brune and Whitney, 2000).

Figure 13b shows the annual probabilities of failure for these four fragility models as a function of time before present, using the mean hazard curve from the 1998 Yucca Mountain PSHA. These annual failure probabilities are computed using the same approach as equation (1) earlier, but the

fragility function now also depends on time t as well as z (the level of PGV) so we denote it $P(G_{\text{fails}}|\text{PGV} = z, t)$

$$P_{\text{annual}}(G_{\text{fails}}(t)) = \sum_i P(G_{\text{fails}}|\text{PGV} = z_i, t)$$
$$\times P_{\text{annual}}(\text{PGV} = z_i). \quad (11)$$

We see in Figure 13b that model 3 failure probabilities are constant for the past 70 ka and drop to zero before then (in its "immovable" state). Model 4 shows the same form but drops to zero before 15 ka. Models 1 and 2 have very low probabilities of failure until ~100 ka, when the probabilities begin to increase noticeably. Failure probabilities for model 1 are always higher than for model 2 because its $\log PGV_{50}$ is always lower until both models become the same at 15 ka.

Given these annual failure probabilities, we can compute the probability of the feature surviving to the present day. The annual probability of surviving is one minus the probability of failure, and the probability of surviving all years is the product of these survival probabilities

$$P(G_{\text{not failed}}) = \prod_{t=1}^{T} \{1 - P_{\text{annual}}[G_{\text{fails}}(t)]\}. \quad (12)$$

Note that the earlier equation (3) is a special case of this equation, when the annual probability of failure is constant rather than changing with t.

To find a corresponding unexceeded ground motion, we again move the hazard curve down by a factor α, which will reduce all of the annual failure probabilities by the same factor α, until the probability of nonfailure in equation (12) is 5%

$$0.05 = \prod_{t=1}^{T} \{1 - \alpha_{0.05} P_{\text{annual}}[G_{\text{fails}}(t)]\}. \quad (13)$$
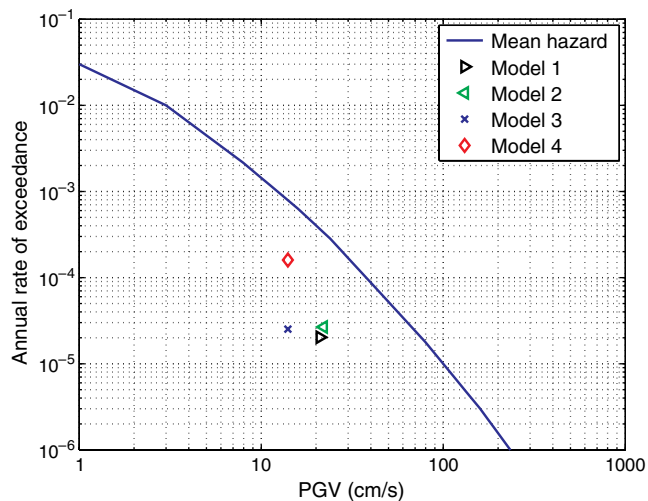
Figure 14. Comparison of the unexceeded ground motions for the four time-dependent fragility models. The color version of this figure is available only in the electronic edition.

Additionally, we need to find the median of the PGVs associated with failure of the feature over its lifetime and again denote this z_1. We then plot the unexceeded ground motion at ordinate z_1 and at the height of the hazard curve shifted down by the factor α determined from equation (13). Figure 14 shows plots of the UGMs obtained using this approach for each of the four time-dependent models.

Several observations can be made regarding the results shown in Figure 14. The model 4 UGM is plotted at a higher rate than the other models' UGMs because the short lifetime assumed in this model means that the hazard would not need to reduce as significantly (i.e., α would not need to be so small) for the feature to have a 5% probability of surviving. This matches our intuition, as the short lifetime should provide a weaker constraint on ground-motion hazard. Models 1 and 2 have z_1 values for PGV that are larger than for models 3 and 4, because in models 1 and 2 the feature is less precarious for most of its lifetime, and failures of the feature in its less precarious state are associated with larger PGV values on average. Finally, models 1 and 2 produce nearly identical locations for the resulting UGM, indicating that the choice of the linear or quadratic decrease in fragility for these models is not a model parameter that significantly affects constraints on hazard. These specific conclusions are not necessarily general to all fragile geologic features, but they illustrate the types of studies that are facilitated by this approach.

Numerical Results for Yucca Mountain Seismic Hazard

The techniques outlined above have been used to compute UGMs at Yucca Mountain for a variety of fragile geologic structures. Shown in Figure 15 are the unexceeded ground motions for the lithophysal units and five precariously balanced rocks computed relative to the mean 1998 Yucca Mountain PGV hazard. Also shown are fractiles of the PGV hazard curves from the 1998 Yucca Mountain PSHA. Each precarious rock is noted several times in the plot, using UGMs corresponding to upper and lower bounds on estimated ages and fragilities of the rock.

The 1998 mean hazard results are inconsistent with survival of the lithophysal units and PBRs in an undamaged state, as evidenced by the location of their UGM points below the mean hazard curve. Although there is some uncertainty in the fragilities and ages of these structures, the 5% survival probabilities of these fragile geologic structures sit well below the 1998 mean hazard. Whereas both the lithophysal units and PBRs support the same conclusion, it is notable that they constrain nonoverlapping portions of the hazard curve. The PBRs provide constraints at exceedance rates of 10^{-5}/yr to 2×10^{-4}/yr and PGVs of 10–30 cm/s, whereas the lithophyse constraints are two orders of magnitude lower in exceedance rate and one order of magnitude larger in PGV value.

The most likely explanation for the discrepancies is that the ground-motion prediction models available in 1998 predicted larger peak ground velocities than modern models developed in the past few years (i.e., Power *et al.*, 2008). Both median predictions and standard deviations of predictions have decreased in the latest models, and it appears that hazard analysis performed with these new models would produce lower hazard curves for Yucca Mountain that are more consistent with the geological evidence considered here. Although these fragile geologic features appear to be inconsistent with the mean hazard curve, this is less clearly the case for the 5th and 15th percentiles of the hazard curves, indicating that some branches of the 1998 Yucca Mountain logic tree produced predictions of ground-motion hazard that are consistent with existence of these fragile geologic features.

Discussion

The results from the above calculations can be compared to earlier estimates produced for the same features with more *ad hoc* approaches. An earlier method used to compute UGMs was to take the ground-motion value (x axis) as the PGV with a 95% chance of failing the FGS (determined from, e.g., Figure 3), and the rate of exceedance (y axis) was the inverse of the age of the FGS (Hanks *et al.*, 2006). This simplified approach was used as a rough check of the consistency of the UGMs and the hazard curves. Figure 16 shows a partial comparison of UGMs computed using this older approach ("old estimate") and the approach proposed here ("new estimate") for the above two example fragile geologic structures at Yucca Mountain. The new estimate of the Matt-Cubed UGM is taken from the Model 3 result in Figure 14; the old estimates for this feature were produced at a time when there was greater uncertainty about the age and fragility of the PBR, so six UGM points were produced then and all are shown in Figure 16. For the Lithophyse, the same LMT fragility curve from Figure 3 was used in both cases; the old
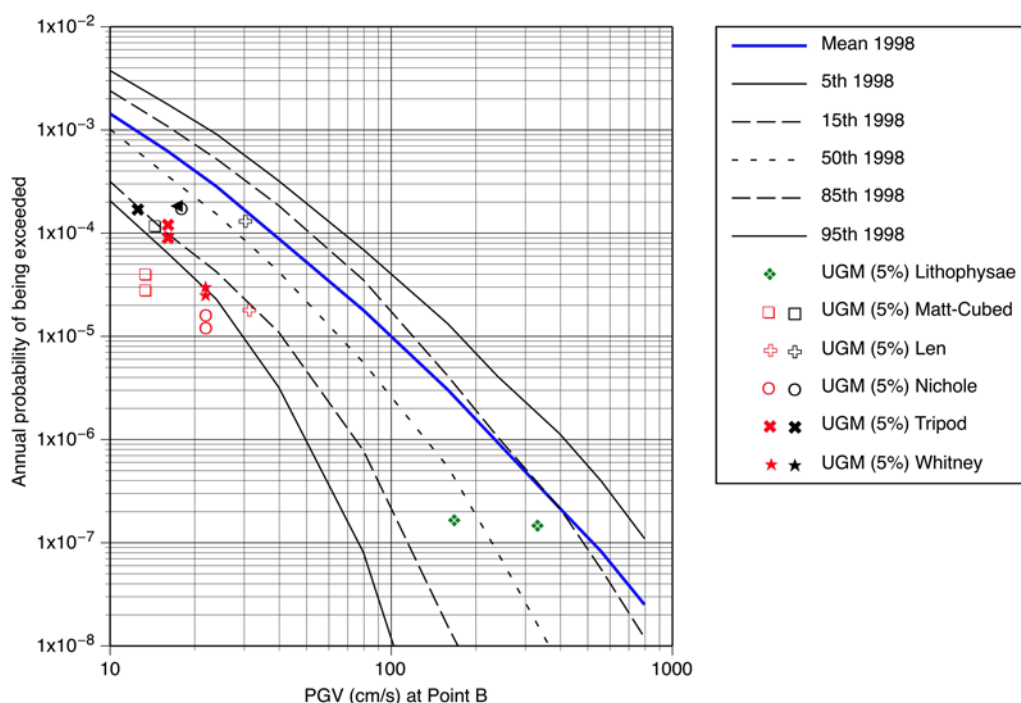
Figure 15. Unexceeded ground motions (UGM) for the lithophysal units and precarious rocks at Yucca Mountain. The color version of this figure is available only in the electronic edition.
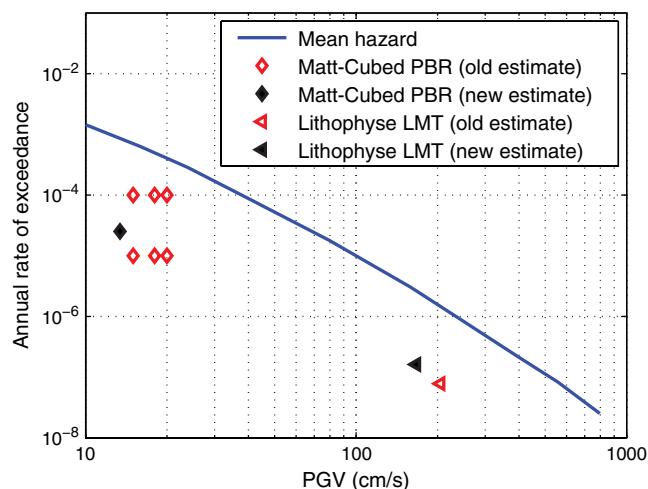
Figure 16. Impact of analysis procedure on plotted location of unexceeded ground motions. The color version of this figure is available only in the electronic edition.

estimate was produced using the simplified approach, whereas the new estimate is taken from Figure 4. The new approach does not significantly change the UGM locations in these two cases, although this is an incomplete comparison of the larger set of data from Yucca Mountain. In this case, both sets of estimates indicate that the fragile geologic structures are incompatible with the 1998 Yucca Mountain mean hazard curve. In cases where the compatibility of fragile geologic structures with a hazard curve is less clear, the proposed procedure will be useful in providing a quantitatively interpret-

able UGM and facilitating the study of how the time-evolving history of a feature affects its compatibility with the computed hazard.

Another item related to interpretation of these results is the specified probability target associated with the UGM. It should be noted that the 5% probability of survival number used to compute UGMs is not intended to indicate the most probable location of the hazard curve as implied by the feature, but rather to indicate a region for which the ground-motion hazard curve is inconsistent with the presence of the observed feature. The 5% probability used above has its origin in statistical hypothesis testing (e.g., Hogg and Tanis, 2009). This test begins with an initial "null hypothesis," which in this example is that the ground-motion hazard at Yucca Mountain is correctly represented by the 1998 PSHA curve. Then new information (in this case the presence of an FGS) is examined to determine whether it is consistent or inconsistent with that null hypothesis. Implied small probabilities of survival of a feature that has in reality survived serve to raise suspicion that the null hypothesis is not in fact correct. Hypothesis testing tradition suggests (somewhat arbitrarily) that observational evidence with $<5\%$ probability of existing under the null hypothesis is sufficient to reject the hypothesis (i.e., to state that the 1998 hazard curve is not consistent with the new information). Other probability values such as 1% or 10% are also used in hypothesis testing and could be easily adopted to compute UGMs if desired. This procedure is a one-way comparison: it looks for evidence of contradiction with the initial hypothesis and does not look for evidence of a match. Although the procedure

is not without flaws, it is an informative test and is used widely in other fields.

This approach has three notable implications for the interpretation of results. First, the location of the UGMs is not intended to indicate the most likely location of an alternative ground-motion hazard curve based on the FGS; it is intended to indicate whether a prior hazard curve is at a location where one could reject its reasonableness using hypothesis testing. Second, the 5% probability threshold is used to indicate inconsistency of the observation with the hazard curve; it does not relate to an implied fraction of surviving FGSs out of some original population of FGSs. Third, this 5% probability applies only to the probability of a single feature surviving. In the case of Yucca Mountain, the fact that ~100 FGSs have been found implies that the probability of the initial hypothesis being true is even smaller. Computation of the exact probability of many features surviving is possible in principle, but there are several significant practical challenges that may not be worth the effort of addressing at that site, given the strong evidence provided by considering the structures individually.

Conclusions

The calculations described here facilitate the quantitative comparison of fragile geologic structures to ground-motion hazard curves obtained from PSHA. Given a structure, with a fragility function that specifies its failure probability as a function of ground-motion intensity and an age or evolutionary model, one can compute a corresponding UGM that can be plotted relative to a ground-motion hazard curve. This approach allows one to make meaningful statistical interpretations using the location of a UGM relative to the hazard curve. The key metric considered is the probability that the feature would have survived to the present day, assuming that the current hazard curve is correct. If the feature has a low probability of having survived, which would be inconsistent with the existence of the feature, then the UGM illustrates how the hazard curve would have to be adjusted to result in a nonnegligible probability of survival.

The proposed calculation approach was initially illustrated for a feature the fragility of which was a function of only a single ground-motion parameter (PGV) and the age of which was clearly defined. The approach was then generalized to consider features with fragility functions that are dependent on a vector of multiple ground-motion parameters, as well as features that slowly evolved to their current fragile state. With these generalizations, a wide range of geologic evidence is able to be compared to hazard analysis results.

Using this approach, the fragility function or time-dependent fragility evolution model can be varied in order to understand sensitivity of the UGM to the feature's assumed properties. The model for time-varying fragility evolution was studied for the example case of a precarious rock at Yucca Mountain, and it was observed that the resulting UGM was relatively insensitive to changes in the evolutionary model. Further experience is needed to draw more general conclusions, but the example calculations presented here demonstrate the potential of this approach to facilitate such studies. Determining the fragilities and ages of fragile geologic features is a sophisticated and time-consuming process, subject to poorly understood uncertainty. The quantification of FGS properties has advanced significantly in recent years, and as refinements in this area continue, the analysis approaches proposed above are useful for utilizing these data for hazard analysis. Further, the calculations above quantify the sensitivity of the hazard constraint to uncertainty in the feature's fragility and age, so that resources can be prioritized for measuring the properties that provide the most useful constraints on hazard.

For seismic hazard analyses where ground-motion amplitudes with very low exceedance rates are of interest (e.g., nuclear facilities and nuclear waste repositories), there has to date been limited ability to validate or constrain hazard results. The unexceeded ground motions indicated by fragile geologic structures are potentially the only way to directly validate seismic hazard curves at such low exceedance rates, but any validation effort needs to be performed with comparable rigor and attention to uncertainty as was used to perform the initial hazard analysis. The procedures described above satisfy that need and should facilitate validation efforts for future seismic hazard calculations.

Data and Resources

All data used in this paper came from published sources listed in the references.

Acknowledgments

References

Abrahamson, N. A., and J. J. Bommer (2005). Probability and uncertainty in seismic hazard analysis, *Earthq. Spectra* **21,** no. 2, 603–607.

Abrahamson, N. A., and T. C. Hanks (2008). Points in hazard space; a new view of PSHA, *Seismol. Res. Lett.* **79,** 285.

Anderson, J. G., and J. N. Brune (1999). Methodology for using precarious rocks in Nevada to test seismic hazard models, *Bull. Seismol. Soc. Am.* **89,** no. 2, 456.

Anderson, J. G., J. N. Brune, G. Biasi, A. Anooshehpoor, and M. Purvance (2011). Workshop report: Applications of precarious rocks and related fragile geological features to U.S. national hazard maps, *Seismol. Res. Lett.* **82,** no. 3, 431–441.

Andrews, D. J., T. C. Hanks, and J. W. Whitney (2007). Physical limits on ground motion at Yucca Mountain, *Bull. Seismol. Soc. Am.* **97,** no. 6, 1771–1792.

Balco, G., M. D. Purvance, and D. H. Rood (2011). Exposure dating of precariously balanced rocks, *Quaternary Geochronol.* **6,** nos. 3–4, 295–303.

Bechtel SAIC Company (BSC) (2005). Peak ground velocities for seismic events at Yucca Mountain, *Nevada. ANL-MGR-GS-000004 REV 00*, Las Vegas, Nevada.

Bell, J. W., J. N. Brune, T. Liu, M. Zreda, and J. C. Yount (1998). Dating precariously balanced rocks in seismically active parts of California and Nevada, *Geology* **26,** no. 6, 495.

Bommer, J., N. Abrahamson, F. O. Strasser, A. Pecker, P.-Y. Bard, H. Bungum, F. Cotton, D. Fah, S. Sabetta, F. Scherbaum, and J. Studer (2004). The challenge of defining upper bounds on earthquake ground motions, *Seismol. Res. Lett.* **75,** 82–95.

Brune, J. N. (1996). Precariously balanced rocks and ground-motion maps for southern California, *Bull. Seismol. Soc. Am.* **86,** no. 1A, 43–54.

Brune, J. N., and J. W. Whitney (1992). Precariously balanced rocks with rock varnish—Paleoindicators of maximum ground acceleration, *Seismol. Res. Lett.* **63,** no. 1, 21.

Brune, J. N., and J. W. Whitney (2000). Precarious rocks and seismic shaking at Yucca Mountain, Nevada., in *Geologic and Geophysical Studies of Yucca Mountain, Nevada, A Potential High-Level Radioactive-Waste Repository*, J. W. Whitney and W. R. Keefer (Editors), USGS Digital Data Series 058, Chapter M, 19 p.

Brune, J. N., D. von Seggern, and A. Anooshehpoor (2003). Distribution of precarious rocks at the Nevada Test Site: comparison with ground motion predictions from nuclear tests, *J. Geophys. Res.* **108,** no. B6, 2306.

Chiou, B., R. Darragh, N. Gregor, and W. Silva (2008). NGA project strong-motion database, *Earthq. Spectra* **24,** no. 1, 23–44.

Hanks, T. C., and N. Abrahamson (2008). A brief history of extreme ground motions, *Seismol. Res. Lett.* **79,** 282–283.

Hanks, T. C., N. A. Abrahamson, M. Board, D. M. Boore, J. N. Brune, and C. A. Cornell (2006). Report of the workshop on extreme ground motions at Yucca Mountain, August 23–25, 2004, *U.S. Geol. Surv. Open-File Rept. 2006-1277*, Reston, Virginia.

Hogg, R. V., and E. Tanis (2009). *Probability and Statistical Inference*, Prentice Hall, Upper Saddle River, New Jersey, 648 pp.

Lockner, D. A., and C. A. Morrow (2008). Energy dissipation in Calico Hills tuff due to pore collapse, *American Geophysical Union*, Fall Meeting, abstract #T51A-1856, San Francisco, California.

McGarr, A., and J. B. Fletcher (2007). Near-fault peak ground velocity from earthquake and laboratory data, *Bull. Seismol. Soc. Am.* **97,** no. 5, 1502.

McGuire, R. K. (1995). Probabilistic seismic hazard analysis and design earthquakes: Closing the loop, *Bull. Seismol. Soc. Am.* **85,** no. 5, 1275–1284.

McGuire, R. K., C. A. Cornell, and G. R. Toro (2005). The case for using mean seismic hazard, *Earthq. Spectra* **21,** no. 3, 879–886.

O'Connell, D. R. H., R. LaForge, and P. Liu (2007). Probabilistic ground-motion assessment of balanced rocks in the Mojave Desert, *Seismol. Res. Lett.* **78,** no. 6, 649–662.

Power, M., B. Chiou, N. Abrahamson, Y. Bozorgnia, T. Shantz, and C. Roblee (2008). An overview of the NGA project, *Earthq. Spectra* **24,** no. 1, 3–21.

Purvance, M., R. Anooshehpoor, and J. N. Brune (2009). Fragilities of Sensitive Geological Features on Yucca Mountain, Nevada, *PEER Report 2009*, University of California, Berkeley, California, 68 p.

Purvance, M. D., J. N. Brune, N. A. Abrahamson, and J. G. Anderson (2008). Consistency of precariously balanced rocks with probabilistic seismic hazard estimates in southern California, *Bull. Seismol. Soc. Am.* **98,** no. 6, 2629–2640.

SSHAC (1997). Recommendations for probabilistic seismic hazard analysis: guidance on uncertainty and use of experts, *U.S. Nuclear Regulatory Commission Report, NUREG/CR-6372*, Washington, D.C.

Stepp, J., I. Wong, J. Whitney, R. Quittemeyer, N. Abrahamson, G. Toro, R. Youngs, K. Coppersmith, J. Savy, and T. Sullivan (2001). Probabilistic seismic hazard analyses for ground motions and fault displacements at Yucca Mountain, Nevada, *Earthq. Spectra* **17,** 113–151.

Stirling, M. W., and R. Anooshehpoor (2006). Constraints on probabilistic seismic-hazard models from unstable landform features in New Zealand, *Bull. Seismol. Soc. Am.* **96,** no. 2, 404–414.

Stirling, M., J. Ledgerwood, T. Liu, and M. Apted (2010). Age of unstable bedrock landforms southwest of Yucca Mountain, Nevada, and implications for past ground motions, *Bull. Seismol. Soc. Am.* **100,** no. 1, 74–86.

Stanford University
473 Via Ortega
MC 4020
Stanford, California 94305
(J.W.B.)

Pacific Gas & Electric Co.
245 Market Street
San Francisco, California 94117
(N.A.A.)

U.S. Geological Survey
P.O. Box 25046
Denver, Colorado 80225
(J.W.W.)

Itasca Consulting Group, Inc.
111 Third Avenue South
Minneapolis, Minnesota 55401
(M.P.B.)

U.S. Geological Survey
345 Middlefield Road MS 977
Menlo Park, California 94305
(T.C.H.)